

TexRO: Generating Delicate Textures of 3D Models by Recursive Optimization

Jinbo Wu, Xing Liu, Chenming Wu, Xiaobo Gao, Jialun Liu, Xinqi Liu, Chen Zhao, Haocheng Feng, Errui Ding, and Jingdong Wang

Department of Computer Vision Technology (VIS), Baidu Inc.

Abstract. This paper presents TexRO, a novel method for generating delicate textures of a known 3D mesh by optimizing its UV texture. The key contributions are two-fold. We propose an optimal viewpoint selection strategy, that finds the most miniature set of viewpoints covering all the faces of a mesh. Our viewpoint selection strategy guarantees the completeness of a generated result. We propose a recursive optimization pipeline that optimizes a UV texture at increasing resolutions, with an adaptive denoising method that re-uses existing textures for new texture generation. Through extensive experimentation, we demonstrate the superior performance of TexRO in terms of texture quality, detail preservation, visual consistency, and, notably runtime speed, outperforming other current methods. The broad applicability of TexRO is further confirmed through its successful use on diverse 3D models. Project page: <https://3d-aigc.github.io/TextRO>.

Keywords: Texture Generation · Multi-View Diffusion

1 Introduction

3D content creation is a vital component in various applications, such as generating visual content for movies, games, and the AR/VR industry. Generative static 3D content creation encompasses two crucial domains of research: the development of high-fidelity geometries and the creation of visually captivating textures. Both tasks share a common objective of democratizing 3D content creation. In recent years, significant advancements have been made in 3D geometry generation, leading to remarkable enhancements in high-quality and diversity [7, 17, 22, 54]. Conversely, the controllable creation of detailed and delicate textures for 3D models remains a challenging area [2, 4, 6, 34].

Recently, diffusion models have made remarkable strides in image generation, largely due to training with abundant data from the Internet. Naturally, one might consider utilizing a 3D diffusion model, trained on 3D textured data, to generate textures (and shapes) within a volumetric 3D space, mirroring the operation of a 2D diffusion model. However, this leads to less effective learning and often produces blurry outcomes [25, 28]. Moreover, regardless of the optimization using efficient latent representations [3], training a 3D diffusion model to a

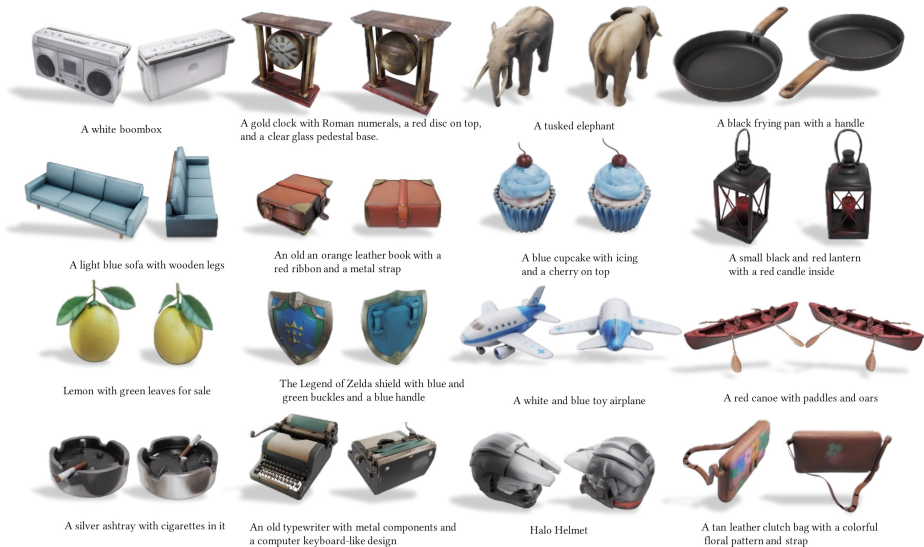


Fig. 1: The proposed TexRO generates realistic textures for a known 3D mesh based on prompts. Our key contributions include: 1) a novel recursive optimization method that refines UV textures at increasing resolutions using the proposed interlaced denoising module, and 2) an effective viewpoints selection strategy. The proposed TexRO has achieved the fastest texture generation (~ 1 min.) and the highest generation quality (as measured by FID and KID scores) compared to previous studies. Example results are showcased in the figure.

satisfactory level requires a significant amount of 3D data and extensive computational resources. An alternative approach involves using distillation sampling to optimize 3D fields [32, 45]. However, these methods often bear the disadvantage of lengthy optimization time, ranging from tens of minutes to hours.

In contrast, we introduce an efficient approach called TexRO for generating realistic textures for a given 3D model. The proposed approach has two stages. In the first stage, we generate an initial UV texture using a readily available depth-driven 2D diffusion method [35]. This initialization process mitigates the issues posed by other 2D diffusion models that fail to retain multi-view consistency. In addition, we propose an optimal viewpoint selection strategy that finds the most miniature set of views covering all the faces of a fmesh. This strategy ensures the completeness of the generated textures. In the second stage, we propose a recursive optimization scheme, where an “adaptive denoising” strategy is employed to optimize the textures. This strategy is capable of re-using existing textures to generate new textures by adaptively injecting noises into pixels with different schedulers. Overall, the recursive optimization scheme optimizes a UV texture at increasing resolutions in RGB space. This design is proposed based on the insight that optimizing a UV texture at a low resolution facilitates generating consistent content while doing so at a high resolution produces details.

Our proposed approach is empirically validated to be robust against changes in rendering view, including alterations in position and orientation.

We conduct extensive experiments on widely-used 3D datasets to validate the effectiveness and efficiency of our proposed method. The results of our experiments manifest that our method can generate textures that maintain global coherence and exhibit intricate details. These textures align well with the conditioning text prompts, as exemplified in Fig 1. The quantitative data indicate that our method significantly advances texture generation for 3D models. Additionally, the qualitative results further corroborate this conclusion. The key contributions of our work can be summarized as follows:

- We introduce *TexRO*, a recursive optimization-based approach, combined with an adaptive denoising method for faster, realistic texture synthesis on 3D geometries leveraging the advancements of pre-trained 2D diffusion models.
- We propose an optimal viewpoint selection strategy to confine an effective optimization space for our proposed recursive optimization.
- Comprehensive experiments and user studies are undertaken to demonstrate our method surpasses existing approaches and represents the cutting edge of current capabilities.

2 Related Work

2.1 Texture Synthesis

Image-based Texture Synthesis has been studied for several decades. Waechter et al. [43] present a comprehensive framework for automatic texturing of large-scale 3D reconstructions from images. It addresses challenges like varying image properties, occluders, and geometry inaccuracies. A graph-cut labeling approach selects optimal textures, followed by global and local color adjustment steps. Zhou et al. [55] addresses the problem of creating colored 3D models using consumer depth cameras, an energy function based on photo-consistency, smoothness, and visibility, is optimized efficiently using belief propagation. Fu et al. [10] first selects an optimal image for each model face, and then performs global camera pose optimization and local texture coordinate refinement to align textures across faces. Huang et al. [18] learns a discriminator as a patch-based misalignment-tolerant metric to guide texture optimization and make it robust to errors in geometry and camera poses. Thies et al. [41] interprets high-dimensional neural textures, which store more information than traditional textures and are capable of handling imperfect 3D content. Yariv et al. [50] and Tang et al. [40] optimize a hybrid neural volume-surface model designed for surface reconstruction, then extract a mesh and an appearance texture for real-time rendering.

Example-based Texture Synthesis primarily involves applying exemplary patterns across a surface, frequently employing a distinct direction field to dictate local orientation, has been well-studied in the computer graphics community. Example-based texture synthesis enables easy content creation and shows

promise for bridging procedural and by-example texturing [46], such as [21] transforms a texture exemplar into an appearance space before synthesis to improve quality and enable new functionalities, [20] extends 2D texture optimization methods to 3D while integrating global histogram matching to improve synthesis quality and convergence. Gatys et al. [12] utilize image latent features extracted by convolutional networks to synthesize textures. GANs have also been explored in [33, 56] to generate more realistic example-based texture outputs. Recently, NeRF-Texture [19] leverages a texture generation network along with the radiance field to synthesize high-quality textures, overcoming the limitations of NeRFs in modeling complex textures.

2.2 Learning to Generate Textures

There exist several works that generate textures in 3D space or field. Texture-Field [28] represents texture as a continuous 3D function parameterized by a neural network. Any 3D point can be mapped to an RGB color value, and this process can be integrated with various shape representations, such as voxels, point clouds, or meshes. EG3D [3] introduces a novel hybrid explicit-implicit network architecture that improves computational efficiency and image quality without relying heavily on approximations. RODIN [44] addresses the computational and memory-intensive nature of high-quality 3D avatar generation by projecting multiple 2D feature maps onto a single plane for efficient 3D-aware diffusion. 3DGen [13] comprises a Variational Autoencoder (VAE) that encodes a colored point cloud into a triplane Gaussian latent space and reconstructs the textured mesh from this latent space and a diffusion model that generates the triplane features. Dundar et al. [9] design a generative adversarial network in UV space to add realistic fine details to texture maps initialized by differentiable rendering, with an attention mechanism in the generator and a learnable position embedding in the discriminator. Sin3DM [47] proposes a novel diffusion model that learns from a single 3D textured shape to generate high-quality variations with detailed geometry and texture using a similar triplane representation. Point-UV Diffusion [51] employs a denoising diffusion model and UV mapping to generate 3D consistent textures, where the semantics of a UV parameterization is an important factor towards high-quality results. Our work leverages a potent pre-trained 2D diffusion model, absent in the 3D realm, and optimizes directly within the color space, as opposed to a 3D space or field, to yield more captivating outcomes in rendered views.

A body of research [1, 5, 6, 14, 23, 29, 31, 42, 48, 49] studies texture generation on a template or aligned space, those methods are prone to lose details or fail to capture the shapes with complex structure or topology. To enable texture generation for more general 3D models, Texturify [36] uses differentiable rendering and adversarial losses to learn high-quality surface texturing from real-world images. Latent-NeRF [25] propagates gradients from a pre-trained 2D diffusion model through differentiable rendering to optimize the latent texture map. TextFusion [2] leverages latent diffusion models, applies a denoiser on a set of 2D renders of the 3D object, and aggregates the denoising predictions on a shared

latent texture map. TEXTure [34] and Paint3D [52] also uses a pre-trained depth-to-image diffusion model to paint a 3D model from different viewpoints, while addressing inconsistencies through a trimap partitioning of the rendered image. Text2Tex [4] also uses a pre-trained depth-aware image diffusion model to synthesize high-resolution partial textures from multiple viewpoints progressively. To avoid inconsistencies and artifacts, the authors introduce a generation mask and an automatic view sequence generation scheme. Distinct from prior research, our work proposes a multiview optimization scheme, employing view optimization to limit the optimizing space. This approach bolsters the quality and multiview consistency of the textures generated.

3 Preliminaries and Problem Definition

Preliminary: Image Diffusion Models. A forward diffusion process is defined as gradually adding noises to an image until it becomes noisy. A diffusion model learns the reversed process for each step. Consequently, the model learns the underlying data distribution, enabling it to generate images. Let $p_\theta(\mathbf{x})$ denote the data distribution and \mathbf{x}_0 represent a data sample. The transformation process models \mathbf{x}_0 as a noisy version of a Gaussian random variable x_T , which can be formulated as $\mathbf{x}_t = \sqrt{1 - \alpha_t} \mathbf{x}_{t-1} + \sqrt{\alpha_t} \boldsymbol{\epsilon}_t$, where $\boldsymbol{\epsilon}_t \sim \mathcal{N}(0, \mathbf{I})$ and $0 \leq \alpha_t \leq 1$ controls the noise level [16]. This process is governed by a stochastic differentiable equation (SDE) that can be discretely approximated over time steps $t = 0, 1, \dots, T$ [38]. To generate new samples, we reverse these steps, where the transition probabilities $q_\theta(x_{t-1}|x_t)$ are guided by a learned reverse-time SDE, by estimating the noise to remove as $\boldsymbol{\epsilon}_\theta^{(t_i)}$ using network θ , allowing the model to gradually add structure to the noise distribution, resulting in samples from $p_\theta(x)$. We leverage iterative diffusion model sampling with Denoising Diffusion Implicit Models (DDIM) [37]:

$$\begin{aligned} \mathbf{x}_{i-1} = & \sqrt{\alpha_{i-1}} \left(\frac{\mathbf{x}_i - \sqrt{1 - \alpha_i} \boldsymbol{\epsilon}_\theta^{(t_i)}(\mathbf{x}_i)}{\sqrt{\alpha_i}} \right) \\ & + \sqrt{1 - \alpha_{i-1} - \sigma_{t_i}^2} \cdot \boldsymbol{\epsilon}_\theta^{(t_i)}(\mathbf{x}_i) + \sigma_{t_i} \boldsymbol{\epsilon}_{t_i}, \end{aligned} \quad (1)$$

where σ_{t_i} is a variance parameter related to α_i and α_{i-1} . For simplification, we denote $\mathbf{f}_\theta^{(t_i)}(\mathbf{x}_{i-1}|\mathbf{x}_i)$ as the function to obtain \mathbf{x}_{i-1} from \mathbf{x}_i by using DDIM sampling.

Preliminary: Mesh and Differentiable Rasterization. In the realm of 3D modeling, it is customary to represent objects using discrete polygons. In our research, we utilize the popular triangular mesh, which consists of arranged triangles so that intersecting triangles only share an edge or a vertex. For a triangular mesh $\mathcal{M} = (\mathcal{V}, \mathcal{T})$ consisting of N vertices and M faces, we typically denote the set of vertices as $\mathcal{V} = \{v_1, v_2, \dots, v_N\}$, where each v_i represents the i -th vertex in 3D space. The triangles are denoted as $\mathcal{T} = \{t_1, t_2, \dots, t_M\}$, where each t_i is defined by three vertices forming a triangle. Differentiable rasterization

is primarily utilized to generate pixel-level derivatives for shading computations in graphics processing units at a given camera viewpoint c . Each vertex v_i in the mesh \mathcal{M} is attributed with distinct properties such as position, color, and texture coordinates in the UV space, where the UV space (u, v) is a parameter space that maps a 2D texture I onto 3D models. Each triangle t_l is subsequently rasterized into a set of fragments $\mathcal{F} = \{f_1, f_2, \dots, f_p\}$ on the imagery plane of camera c , we denote this process as $\mathcal{R}(\cdot)$ and its reverse process as $\hat{\mathcal{R}}(\cdot)$. For each fragment f_j , the attributes at that point are interpolated from the attributes of the vertices of the triangle t_l that the fragment belongs to, including the UV coordinates, which are used to look up the corresponding texture color.

Problem Definition. Having established the necessary preliminaries and notations, we formally define the problem addressed in our research. We consider an input triangular mesh \mathcal{M} and a textual prompt p . The objective is to generate a UV texture \mathbf{y} that aligns with the semantics of p using a 2D image diffusion model and differentiable rasterization from viewpoints $\{C_n\}$. Our goal is to ensure that the resulting images, obtained by mapping the texture I from the UV space to the intrinsic surface space of the mesh \mathcal{M} , not only exhibit high perceptual quality and consistency with p , but also maintain multiview consistency. It is essential for this consistency to hold even under novel view conditions, extending beyond the optimization of any pair of views from the set $\{C_n\}$.

4 Method

The proposed TexRO generates multi-view consistent and high-quality textures for 3D objects by optimizing its UV texture. TexRO’s pipeline consists of two stages. In the first stage, we propose an effective viewpoint selection strategy that finds the smallest set of viewpoints covering a mesh’s faces. In addition, we synthesize multi-view images for the given mesh and project the colors to the UV texture map to establish an initial status of the UV texture for later optimization. In the second stage, we recursively optimize the UV texture with an increasing resolution in RGB space. Specifically, we first optimize the UV texture using the proposed adaptive denoising strategy under the selected views at a low resolution, then we upsample the UV texture map and conduct the same optimization to achieve a better quality of textures at a higher resolution. We repeat this recursive process N times. This design is made based on our insight that optimizing a UV texture with nearest neighbor sampling at a low resolution facilitates generating consistent content while doing so at a high resolution produces details. Our recursive optimization is thus capable of generating consistent and detailed textures. It is noteworthy that the proposed recursive optimization operates in RGB space, which ensures an accurate UV mapping during the optimization. In the following sections, we introduce the proposed modules in detail. We first introduce the proposed view selection strategy in Sec. 4.1, then we introduce the proposed recursive optimization pipeline in Sec. 4.2.

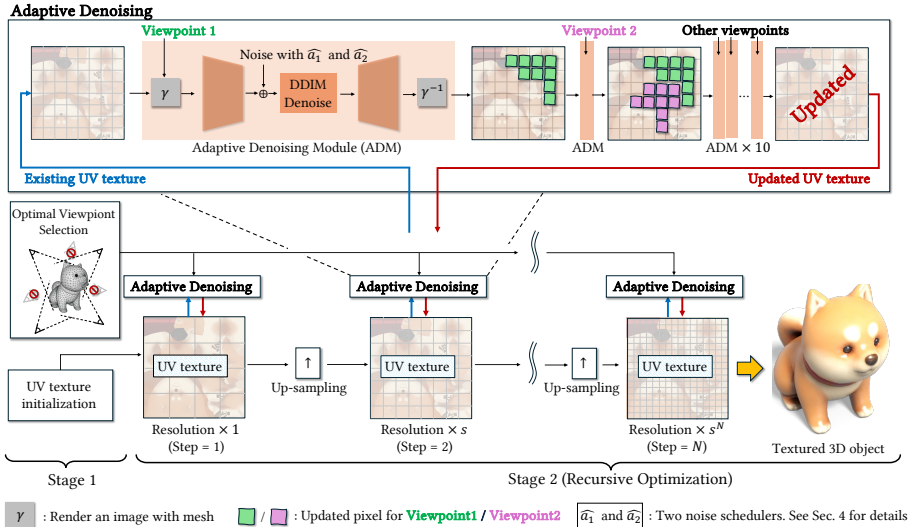


Fig. 2: The outline of the proposed TexRO is illustrated in the figure. It has two stages. In stage 1, it produces an optimal set of viewpoints and generates an initial UV texture for later optimization. In stage 2, it conducts the recursive optimization that optimizes the UV texture at increasing resolutions. The details of the proposed adaptive denoising strategy is illustrated at the top of the figure. $\hat{\alpha}_1$ and $\hat{\alpha}_2$ are two noise schedulers.

4.1 Optimal Viewpoints Selection

It is known that a crucial factor influencing the quality of generation is the selection of viewpoints. Previous studies such as [2, 34] employed a predefined set of candidate viewpoints; Text2Tex [4] attempted to optimize the view set but still rely on a relatively small number ($= 36$) of candidates accompanied by dynamic gain computation. In this paper, we propose a viewpoints selection strategy that finds the smallest set of views covering all the faces of a mesh. This guarantees the completeness of a generated result. Although a naive approach involves densely surrounding an object with cameras, this strategy significantly increases the optimization time. The proposed strategy formulates the goal as a *Set-Cover Problem (SCP)* [8] and solves it efficiently using a heuristic greedy strategy and further relaxing the 0-1 integer programming problem of minimal coverage to a general optimization problem of maximizing the sum of areas of all covered faces. In the supplementary material, we provide a detailed explanation of the algorithm and its implementation details. Table 2 validates the effectiveness of the proposed viewpoints selection method.

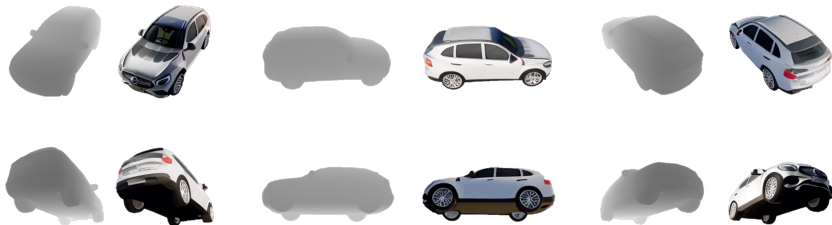


Fig. 3: We employ depth-controlled Zero123Plus [35] for our UV texture map initialization. The prompt for generating this example is “a Mercedes-Benz car”.

4.2 Recursive Optimization of UV Texture

Overview. The proposed recursive optimization operates in the RGB space. It synthesizes realistic (consistent&high visual quality) textures from a prompt by optimizing the UV texture at increasing resolutions. As illustrated in Fig. 2, our optimization pipeline consists of N steps. In a step, it optimizes the UV texture using the proposed adaptive denoising strategy and updates the UV texture with the optimized result. Then, it upsamples the UV texture by a factor of s ($= 1.5$) and optimizes it at the increased resolution using the same denoising strategy in the following step. The optimizations conducted at increasing resolutions enable it to progressively generate textural details. Our pipeline recursively conducts the explained processes for N steps to generate final results.

Initialization. The quality of an initial UV texture affects the outcome of the final texture generation, as the proposed adaptive denoising module creates new textures based on existing ones (we introduce this in the following paragraph). We have empirically investigated that the depth-driven Zero123Plus [35] serves as the most appropriate model for our UV texture initialization. This model takes an image rendered from a viewpoint as input and outputs a generated image guided by a depth map that was rendered from another point of view. We employ this model to generate six multi-view images for a mesh and project the colors from these views onto the UV texture map for initialization. Fig. 3 showcases a set of generated results.

Adaptive denoising. We have illustrated the outline of the proposed adaptive denoising operation at the top of Fig. 2, it takes the UV texture and the selected view set as input and incrementally synthesizes textures from all the viewpoints. The key insight of the adaptive denoising strategy lies in re-using the existing textures generated from the last step (or made by the UV texture initialization when $Step = 1$) for generating new textures in the current step. As illustrated in Fig. 4, unlike the straightforward way [4, 34] that generates new textures from pure noise, we inject scheduled noises into the existing textures and refine them by an image-to-image diffusion model. We compute the noises for the overlapping

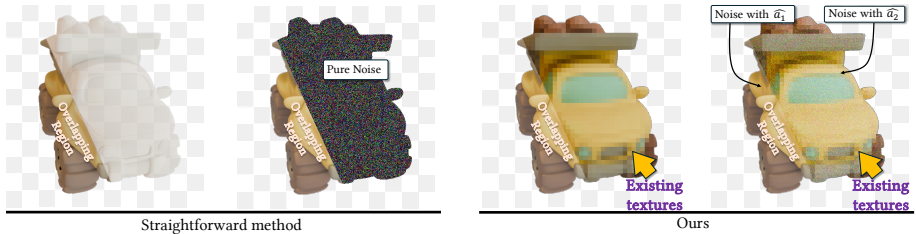


Fig. 4: The key difference between the proposed adaptive denoising strategy and the straightforward method used in the previous studies [4, 34]. In contrast to the straightforward that generates new textures from pure noise using an image inpainting diffusion model, ours injects noises to refine existing textures. We introduce how α_{t_1} and α_{t_2} are computed in Sec. 4.2’s adaptive denoising.

region and the non-overlapping region with different noise schedulers denoted as $\widehat{\alpha}_1$ and $\widehat{\alpha}_2$, using

$$\widehat{\alpha}_1 = \left(\sqrt{\frac{\overline{\alpha_{t_n}}}{\alpha_{t_1}}} z_{n,i} + \sqrt{1 - \frac{\overline{\alpha_{t_n}}}{\alpha_{t_1}}} \epsilon \right), \quad (2)$$

$$\widehat{\alpha}_2 = \left(\sqrt{\frac{\overline{\alpha_{t_n}}}{\alpha_{t_2}}} z_{n,i} + \sqrt{1 - \frac{\overline{\alpha_{t_n}}}{\alpha_{t_2}}} \epsilon \right), \quad (3)$$

where $\overline{\alpha_{t_x}} = \prod_{u=1}^{u=t_x} \alpha_u$, $t_n = 10$, $t_1 = 2$, $t_2 = t_n - 1$. We have practically observed that t_1 has merely a light impact on the generation quality. We discuss the options for t_n in Sec. 5.5. $z_{n,i}$ means the encoded image corresponding to viewpoint i and step n . ϵ is sampled from a normal distribution.

Multi-resolution UV texture. We have claimed that the proposed recursive optimization approach can generate realistic textures. We explain how this is supported by the proposed multi-resolution UV texture design. When generating textures with a low-resolution UV texture, the algorithm can retrieve more pixels from the UV texture for the overlapping region (see the evidence in supplementary material) that guides new texture generation in the adjacent viewpoints. This leads to better content consistency compared with the case where the overlapping region is small. Our design starts with a low-resolution UV texture based on this insight. To address the issue that a low-resolution UV texture can cause blocking artifacts in the generated result, we progressively increase the UV texture’s resolution in the later steps (as shown in Fig. 2). Although such a manner will decrease the number of pixels included in each overlapping region in a later step, content consistency will be maintained because the existing textures used in a later step are already formed with consistent structures. Fig. 5 demonstrates the correctness and effectiveness of the proposed multi-resolution UV texture design. Fig. 5(a) showcases that consistent and high-quality textures are generated with increasing resolutions as we claimed above; Fig. 5(b) demonstrates that the proposed approach which involves multi-resolution UV texture,

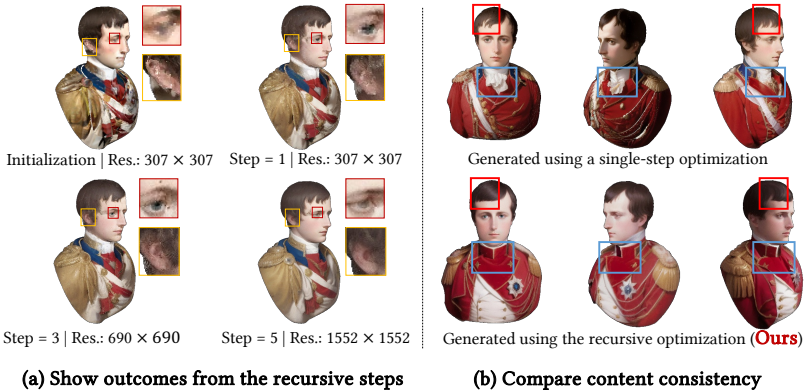


Fig. 5: (a) showcases the outcome of each recursive step in Stage-2, where “initialization” refers to the initial UV texture produced in Stage-1. (b) compares the results from the proposed recursive optimization with those from a single-step optimization performed at the highest resolution (1552×1552), defined as the resolution applied in Step 5 of our method.

generates more consistent results than a single-step optimization conducted at the highest resolution.

5 Experiments

5.1 Implementation Details

We describe the implementation details. In the optimal view selection module belonging to Stage 1, we start finding the optimal set from a collection of 8192 view-point candidates. To produce an initial UV texture, we employ a depth-driven Zero123Plus and six camera poses for synthesizing views. The camera poses are defined in the spherical coordinate system. Specifically, their azimuth angles are $[30, 90, 150, 210, 270, 330]$, and their elevation angles are $[60, 110, 60, 110, 60, 110]$. For the proposed recursive optimization in Stage 2, we set $N = 5$, indicating that the resolutions of UV texture are 307, 460, 690, 1035, and 1552. We employ a depth-driven ControlNet [53] (finetuned from Stable Diffusion v1.5) that performs image restoration to synthesize textures in the proposed adaptive denoising module. We compute t_n for α_{t_n} for a step n using

$$t_n = \max(10 - s \cdot n, 5) \quad (4)$$

where $s = 2.5$ in our experiment. We implemented our method using Python and C++ in a hybrid fashion. We employed PyTorch [30] for implementing most computations. We employed Kaolin [11] for differentiable rendering and texture projection. Our method is capable of generating realistic textures around *only 1 minute*.



Fig. 6: Qualitative comparison of the generated textures among Latent-Paint [25], Text2Tex [4], TEXTure [34] and our proposed TexRO.

5.2 Experiment Setup

Benchmark Dataset. We employ the dataset (namely, *Text2Tex-Data*) provided in Text2Tex [4] for evaluation. In the *Text2Tex-Data*, each sample contains a mesh with textures and a brief caption describing the 3D object (using all categories as captions for objects). We compare the proposed approach and the baseline approaches using the *Text2Tex-Data*. We summarize the evaluation results in Table 1. In addition, we investigate how well the text-to-texture generation methods, including ours and the baselines, can perform when text guidance is detailed. As mentioned, the *Text2Tex-Data* only provided a brief caption for each sample. We thus bring high-quality captions provided with Cap3D [24] into our experiment. The Cap3D’s caption of an object presents more details, such as “A 3D model of a black and white microwave oven with a power cord” about its texture compared to the *Text2Tex-Data*’s. We reform a new evaluation dataset (denoted by *Text2Tex-Cap3d*) by taking the intersection of the *Text2Tex-Data* and the Cap3D dataset. This dataset consists of 310 samples, each consisting of a high-quality mesh with textures and a detailed caption. We conduct the same performance comparison on the *Text2Tex-Cap3d* dataset and summarize the results in Table 2. Some objaverse data visual results can be found in the Fig. 8.

Baselines. We benchmark our method against the following leading-edge text-driven texture synthesis methods: Text2Mesh [26], CLIPMesh [27], Latent-Paint [25], Text2Tex [4] and TEXTure [34]. We omitted TexFusion [2] due to its closed source.

Evaluation Metrics. We employ Fréchet Inception Distance (FID) [15] and Kernel Inception Distance (KID) [39] for evaluating the proposed approach and the baselines. For each test sample, we first synthesize textures using these approaches using the identical mesh and caption. Then, we randomly select 20 camera poses looking toward the object and render images with the synthesized textures. The groundtruth image set needed for computing FID and KID

Table 1: Evaluation results on the commonly used subset of Objaverse, *i.e.*, **Text2Tex-Data**, for 3D texture generation, we add TexFusion results

Methods	FID ↓	KID ($\times 10^{-3}$) ↓	Runtime
Text2Mesh [26]	45.38	10.40	10 min.
CLIPMesh [27]	43.25	12.52	50 min.
Latent-Paint [25]	43.87	11.43	22 min.
TEXTure [34]	39.09	9.97	5 min.
Text2Tex [4]	35.68	7.74	15 min.
TexRO(Ours)	33.83	5.77	1 min.

is rendered using the original texture provided with the dataset and the same 20 camera poses. We use a resolution of 512×512 for all the renderings in our evaluation.

Runtime. One of the strengths of the proposed approach is its ability to generate textures rapidly. It can complete a generation within one minute with a single NVIDIA A100 GPU with 40G VRAM. To demonstrate our superiority, we provide a computation time comparison in Table 1. The numbers in the table validated the effectiveness of our approach.

5.3 Quantitative Comparison

The quantitative results computed on **Text2Tex-Data** are provided in Table 1. The result values for the baseline methods are borrowed from [4]. The table shows that the proposed approach outperforms the baseline methods significantly. Our approach also achieves the shortest computation time. In Table 2, we provide the quantitative results computed on the **Text2Tex-Cap3d** dataset. Due to the limitation of our computing resources, we only compare the proposed approach with the strongest baseline (*i.e.* Text2Tex [4]) on the **Text2Tex-Cap3d** dataset to demonstrate our superior effectiveness. It is seen in Table 1 that the proposed approach outperforms the baseline methods. It is noteworthy that involving detailed captions can improve the quality of texture generation, as we have stated before. See the result values of the proposed approach shown in both Table 1 and Table 2-**TexRO(w/ View Sel.)**.

To further validate the effectiveness of the proposed approach, we conducted a user study for comparison. The user study involved 20 participants who possess fundamental knowledge of 3D modeling. We randomly select 100 samples from the **Text2Tex-Data** and conduct pairwise comparisons. For each sample, we produce two images rendered using the UV texture maps generated from the proposed approach and Text2Tex [4] with an identical camera pose. Consequently, we asked the participants to output pairwise preference for each sample based on overall perceptual quality, which includes 1) multi-view consistency, 2) detail richness, and 3) natural color representation. The results of this user study indicate a clear preference for the proposed approach. Compared to the results of

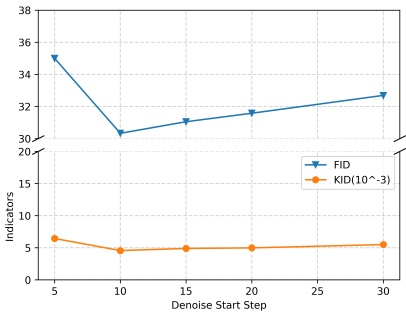


Fig. 7: The impact of distinct denoising step counts on FID and KID.

Table 2: The results are computed on **Text2Tex-Cap3d**. In the left table, TexRO (*w/o* View Sel.) and TexRO (*w/* View Sel.) mean the texture generations without and with the proposed viewpoint selection strategy. In the case of TexRO (*w/o* View Sel.), the viewpoints are uniformly distributed.

Method	FID ↓	KID ($\times 10^{-3}$) ↓
Text2Tex [4]	34.14	5.94
TexRO (<i>w/o</i> View Sel.)	32.75	5.42
TexRO (<i>w/</i> View Sel.)	30.33	4.58

Text2Tex [4], Ours received a favorable verdict, with a preference ratio of 68.4% versus 31.6%. This reinforces the superior quality of the textures generated by our method. We conduct extensive comparisons between our proposed method and [2] and report the results in the supplementary material.

5.4 Qualitative Results

We present our qualitative results in Fig. 1 and Fig. 8. All our renderings are conceived from novel viewpoints, showcasing the versatility and adaptability of our approach. In addition, more visual results are available in Fig. 6 to further evaluate the quality of our generated 3D textures. This visual comparison further emphasizes the level of detail and accuracy achieved by our approach.

5.5 Ablation Study

Effectiveness of view selection. We demonstrate the effectiveness of the proposed optimal view selection by conducting experiments on **Text2Tex-Cap3d**. Table 2 shows the result values computed *w/* and *w/o* the proposed optimal view selection method. It is seen that the proposed method effectively improves the performance of texture generation by 1.70 and $0.56(\times 10^{-3})$ for FID (\downarrow) and KID (\downarrow).

Choices of values for α_{t_n} . We have introduced in Sec. 4.2 that we gradually decrease the noise level with increasing step n_i . We analyze how different starting values of noise level (*i.e.* the noise level at $n_i = 1$) affect texture generation results. We provide quantitative results computed using different starting values of the noise level in Fig. 7. It is seen that 10 gives the best performance compared to other options.

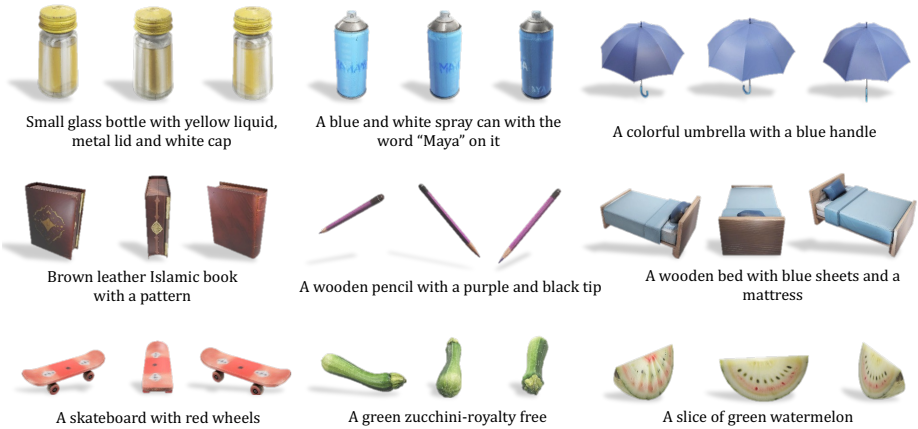


Fig. 8: Additional results generated by our proposed TexRO method using texts as prompts. More results are showed in our supplementary material.

6 Conclusion

We introduce TexRO, a novel method for generating realistic textures on 3D geometries. The key innovations lie in the proposed recursive optimization pipeline and the optimal view selection strategy. The recursive optimization utilizes an interlaced denoising strategy that leverages the advancements in diffusion probabilistic models to synthesize textures at increasing resolutions. This facilitates it to first generate consistent structures, and then enhance details of textures. Through rigorous experimentation and user studies, TexRO has proven to significantly surpass existing methods in delivering superior texture quality, remarkable detail preservation, enhanced visual consistency, and improved runtime efficiency, applicable across various 3D models.

Limitation. While the proposed TexRO demonstrates effectiveness in generating realistic textures for a wide range of 3D models, it encounters two primary limitations. First, it requires the input meshes to be water-tight (2-manifolds), which may limit its applicability to industrial uses, such as repainting objects whose geometry has been reconstructed using photometric methods. Investigating this will be a priority in our future work. Secondly, TexRO occasionally fails to accurately texture areas within meshes that possess complex topologies. We believe that direct optimization on the mesh surfaces could overcome this issue. Lastly, we aim to extend TexR’s capabilities for generating physically-based rendering (PBR) materials, aligning with modern rendering engine standards.

References

1. Bhattad, A., Dundar, A., Liu, G., Tao, A., Catanzaro, B.: View generalization for single image textured 3D models. In: CVPR (2021) [4](#)
2. Cao, T., Kreis, K., Fidler, S., Sharp, N., Yin, K.: Textfusion: Synthesizing 3D textures with text-guided image diffusion models. In: ICCV. pp. 4169–4181 (2023) [1](#), [4](#), [7](#), [11](#), [13](#)
3. Chan, E.R., Lin, C.Z., Chan, M.A., Nagano, K., Pan, B., De Mello, S., Gallo, O., Guibas, L.J., Tremblay, J., Khamis, S., et al.: Efficient geometry-aware 3D generative adversarial networks. In: CVPR. pp. 16123–16133 (2022) [1](#), [4](#)
4. Chen, D.Z., Siddiqui, Y., Lee, H.Y., Tulyakov, S., Nießner, M.: Text2Tex: Text-driven texture synthesis via diffusion models. In: ICCV (2023) [1](#), [5](#), [7](#), [8](#), [9](#), [11](#), [12](#), [13](#)
5. Chen, W., Gao, J., Ling, H., Smith, E., Lehtinen, J., Jacobson, A., Fidler, S.: Learning to predict 3D objects with an interpolation-based differentiable renderer. In: NeurIPS (2019) [4](#)
6. Chen, Z., Yin, K., Fidler, S.: AUV-Net: Learning aligned UV maps for texture transfer and synthesis. In: CVPR. pp. 1465–1474 (2022) [1](#), [4](#)
7. Cheng, Y.C., Lee, H.Y., Tulyakov, S., Schwing, A., Gui, L.: SDFusion: Multimodal 3D shape completion, reconstruction, and generation. In: CVPR (2023) [1](#)
8. Cormen, T.H., Leiserson, C.E., Rivest, R.L., Stein, C.: Introduction to algorithms. MIT press (2022) [7](#)
9. Dundar, A., Gao, J., Tao, A., Catanzaro, B.: FINE detailed texture learning for 3D meshes with generative models. IEEE TPAMI (2023) [4](#)
10. Fu, Y., Yan, Q., Yang, L., Liao, J., Xiao, C.: Texture mapping for 3D reconstruction with RGB-D sensor. In: CVPR. pp. 4645–4653 (2018) [3](#)
11. Fuji Tsang, C., Shugrina, M., Lafleche, J.F., Takikawa, T., Wang, J., Loop, C., Chen, W., Jatavallabhula, K.M., Smith, E., Rozantsev, A., Perel, O., Shen, T., Gao, J., Fidler, S., State, G., Gorski, J., Xiang, T., Li, J., Li, M., Lebedev, R.: Kaolin: A pytorch library for accelerating 3D deep learning research. <https://github.com/NVIDIAGameWorks/kaolin> (2022) [10](#)
12. Gatys, L., Ecker, A.S., Bethge, M.: Texture synthesis using convolutional neural networks. NeurIPS **28** (2015) [4](#)
13. Gupta, A., Xiong, W., Nie, Y., Jones, I., Oğuz, B.: 3DGen: Triplane latent diffusion for textured mesh generation. arXiv preprint arXiv:2303.05371 (2023) [4](#)
14. Henderson, P., Tsiminaki, V., Lampert, C.: Leveraging 2D data to learn textured 3D mesh generation. In: CVPR (2020) [4](#)
15. Heusel, M., Ramsauer, H., Unterthiner, T., Nessler, B., Hochreiter, S.: GANs trained by a two time-scale update rule converge to a local nash equilibrium. NeurIPS **30** (2017) [11](#)
16. Ho, J., Jain, A., Abbeel, P.: Denoising diffusion probabilistic models. In: NeurIPS. vol. 33, pp. 6840–6851 (2020) [5](#)
17. Hong, Y., Zhang, K., Gu, J., Bi, S., Zhou, Y., Liu, D., Liu, F., Sunkavalli, K., Bui, T., Tan, H.: Lrm: Large reconstruction model for single image to 3d. In: ICLR (2024) [1](#)
18. Huang, J., Thies, J., Dai, A., Kundu, A., Jiang, C., Guibas, L.J., Nießner, M., Funkhouser, T., et al.: Adversarial texture optimization from rgb-d scans. In: CVPR. pp. 1559–1568 (2020) [3](#)
19. Huang, Y.H., Cao, Y.P., Lai, Y.K., Shan, Y., Gao, L.: NeRF-Texture: Texture synthesis with neural radiance fields. In: ACM SIGGRAPH. pp. 1–10 (2023) [4](#)

20. Kopf, J., Fu, C.W., Cohen-Or, D., Deussen, O., Lischinski, D., Wong, T.T.: Solid texture synthesis from 2d exemplars. In: ACM SIGGRAPH, pp. 2–es. ACM (2007) [4](#)
21. Lefebvre, S., Hoppe, H.: Appearance-space texture synthesis. ACM TOG **25**(3), 541–548 (2006) [4](#)
22. Li, J., Tan, H., Zhang, K., Xu, Z., Luan, F., Xu, Y., Hong, Y., Sunkavalli, K., Shakhnarovich, G., Bi, S.: Instant3d: Fast text-to-3d with sparse-view generation and large reconstruction model. In: ICLR (2024) [1](#)
23. Li, X., Liu, S., De Mello, S., Kim, K., Wang, X., Yang, M.H., Kautz, J.: Online adaptation for consistent mesh reconstruction in the wild. In: NeurIPS (2020) [4](#)
24. Luo, T., Rockwell, C., Lee, H., Johnson, J.: Scalable 3d captioning with pretrained models. NeurIPS **36** (2024) [11](#)
25. Metzger, G., Richardson, E., Patashnik, O., Giryes, R., Cohen-Or, D.: Latent-NeRF for shape-guided generation of 3D shapes and textures. In: CVPR. pp. 12663–12673 (2023) [1](#), [4](#), [11](#), [12](#)
26. Michel, O., Bar-On, R., Liu, R., Benaim, S., Hanocka, R.: Text2Mesh: Text-driven neural stylization for meshes. In: CVPR. pp. 13492–13502 (2022) [11](#), [12](#)
27. Mohammad Khalid, N., Xie, T., Belilovsky, E., Popa, T.: CLIP-Mesh: Generating textured meshes from text using pretrained image-text models. In: ACM SIGGRAPH Asia. pp. 1–8 (2022) [11](#), [12](#)
28. Oechsle, M., Mescheder, L., Niemeyer, M., Strauss, T., Geiger, A.: Texture fields: Learning texture representations in function space. In: ICCV. pp. 4531–4540 (2019) [1](#), [4](#)
29. Pan, X., Dai, B., Liu, Z., Loy, C.C., Luo, P.: Do 2D GANs Know 3D Shape? unsupervised 3d shape reconstruction from 2d image gans. In: ICLR (2021) [4](#)
30. Paszke, A., Gross, S., Massa, F., Lerer, A., Bradbury, J., Chanan, G., Killeen, T., Lin, Z., Gimelshein, N., Antiga, L., Desmaison, A., Kopf, A., Yang, E., DeVito, Z., Raison, M., Tejani, A., Chilamkurthy, S., Steiner, B., Fang, L., Bai, J., Chintala, S.: Pytorch: An imperative style, high-performance deep learning library. In: NeurIPS, pp. 8024–8035. Curran Associates, Inc. (2019) [10](#)
31. Pavlo, D., Spinks, G., Hofmann, T., Moens, M.F., Lucchi, A.: Convolutional generation of textured 3D meshes. In: NeurIPS (2020) [4](#)
32. Poole, B., Jain, A., Barron, J.T., Mildenhall, B.: Dreamfusion: Text-to-3D using 2D diffusion. In: ICLR (2022) [2](#)
33. Portenier, T., Arjomand Bigdeli, S., Goksel, O.: Gramgan: Deep 3d texture synthesis from 2d exemplars. NeurIPS **33**, 6994–7004 (2020) [4](#)
34. Richardson, E., Metzger, G., Alaluf, Y., Giryes, R., Cohen-Or, D.: TEXTure: Text-guided texturing of 3D shapes. In: SIGGRAPH (2023) [1](#), [5](#), [7](#), [8](#), [9](#), [11](#), [12](#)
35. Shi, R., Chen, H., Zhang, Z., Liu, M., Xu, C., Wei, X., Chen, L., Zeng, C., Su, H.: Zero123++: a single image to consistent multi-view diffusion base model. arXiv preprint arXiv:2310.15110 (2023) [2](#), [8](#)
36. Siddiqui, Y., Thies, J., Ma, F., Shan, Q., Niefner, M., Dai, A.: Texturify: Generating textures on 3D shape surfaces. In: ECCV. pp. 72–88. Springer (2022) [4](#)
37. Song, J., Meng, C., Ermon, S.: Denoising diffusion implicit models. In: ICLR (2020) [5](#)
38. Song, Y., Ermon, S.: Generative modeling by estimating gradients of the data distribution. In: NeurIPS. vol. 32 (2019) [5](#)
39. Sutherland, J., Arbel, M., Gretton, A.: Demystifying mmd gans. In: ICLR. pp. 1–36 (2018) [11](#)

40. Tang, J., Zhou, H., Chen, X., Hu, T., Ding, E., Wang, J., Zeng, G.: Delicate textured mesh recovery from nerf via adaptive surface refinement. In: ICCV (2023) [3](#)
41. Thies, J., Zollhöfer, M., Nießner, M.: Deferred neural rendering: Image synthesis using neural textures. ACM TOG **38**(4), 1–12 (2019) [3](#)
42. Tulsiani, S., Kulkarni, N., Gupta, A.: Implicit mesh reconstruction from unannotated image collections. arXiv preprint arXiv:2007.08504 (2020) [4](#)
43. Waechter, M., Moehrle, N., Goesele, M.: Let there be color! large-scale texturing of 3D reconstructions. In: ECCV. pp. 836–850. Springer (2014) [3](#)
44. Wang, T., Zhang, B., Zhang, T., Gu, S., Bao, J., Baltrusaitis, T., Shen, J., Chen, D., Wen, F., Chen, Q., et al.: Rodin: A generative model for sculpting 3D digital avatars using diffusion. In: CVPR. pp. 4563–4573 (2023) [4](#)
45. Wang, Z., Lu, C., Wang, Y., Bao, F., Li, C., Su, H., Zhu, J.: Prolificdreamer: High-fidelity and diverse text-to-3D generation with variational score distillation. NeurIPS (2023) [2](#)
46. Wei, L.Y., Lefebvre, S., Kwatra, V., Turk, G.: State of the art in example-based texture synthesis. EG pp. 93–117 (2009) [4](#)
47. Wu, R., Liu, R., Vondrick, C., Zheng, C.: Sin3DMM: Learning a diffusion model from a single 3D textured shape. In: ICLR (2024) [4](#)
48. Wu, S., Rupprecht, C., Vedaldi, A.: Unsupervised learning of probably symmetric deformable 3D objects from images in the wild. In: CVPR. pp. 1–10 (2020) [4](#)
49. Xiang, F., Xu, Z., Hasan, M., Hold-Geoffroy, Y., Sunkavalli, K., Su, H.: Neutex: Neural texture mapping for volumetric neural rendering. In: CVPR. pp. 7119–7128 (2021) [4](#)
50. Yariv, L., Hedman, P., Reiser, C., Verbin, D., Srinivasan, P.P., Szeliski, R., Barron, J.T., Mildenhall, B.: Baked sdf: Meshing neural sdfs for real-time view synthesis. arXiv preprint arXiv:2302.14859 (2023) [3](#)
51. Yu, X., Dai, P., Li, W., Ma, L., Liu, Z., Qi, X.: Texture generation on 3D meshes with point-uv diffusion. In: ICCV. pp. 4206–4216 (2023) [4](#)
52. Zeng, X.: Paint3d: Paint anything 3d with lighting-less texture diffusion models. arXiv preprint arXiv:2312.13913 (2023) [5](#)
53. Zhang, L., Rao, A., Agrawala, M.: Adding conditional control to text-to-image diffusion models. In: Proceedings of the IEEE/CVF International Conference on Computer Vision. pp. 3836–3847 (2023) [10](#)
54. Zheng, X.Y., Pan, H., Wang, P.S., Tong, X., Liu, Y., Shum, H.Y.: Locally attentional sdf diffusion for controllable 3D shape generation. ACM TOG **42**(4) (2023) [1](#)
55. Zhou, Q.Y., Koltun, V.: Color map optimization for 3D reconstruction with consumer depth cameras. ACM TOG **33**(4), 1–10 (2014) [3](#)
56. Zhou, Y., Zhu, Z., Bai, X., Lischinski, D., Cohen-Or, D., Huang, H.: Non-stationary texture synthesis by adversarial expansion. arXiv preprint arXiv:1805.04487 (2018) [4](#)

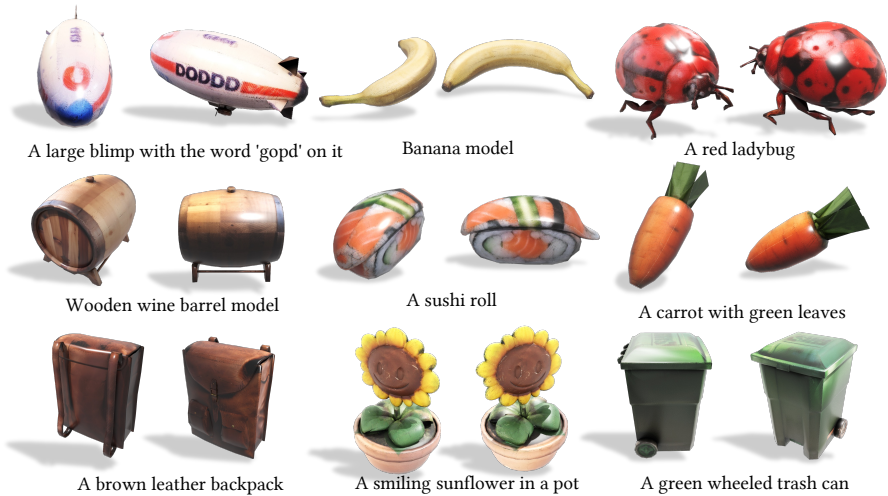


Fig. 8: More results from the proposed TexRO.

7 Implementation Details and Additional Results

Prompt Augmentation We employ prompt augmentation to improve the performance of the stable diffusion models used in our method, following [32]. We add the word “front” when azimuth lies in $[0^\circ, 30^\circ]$ or $[330^\circ, 360^\circ]$ to the original prompt; add the word “back” when azimuth lies in $[30^\circ, 150^\circ]$ or $[210^\circ, 330^\circ]$ to the original prompt.

More results from TexRO We provide more results generated using our TexRO in Fig. 8.

8 Explanation of Optimal Viewpoints Selection

We explain the details of the proposed viewpoints selection algorithm. We have explained in Sec.3-Preliminary of the main text that a 3D mesh is represented by triangle faces. The goal of the proposed viewpoints selection method is to find the smallest set of viewpoints covering all the faces of a mesh.

Lemma 1. *Let U and \mathcal{A} represent two universal sets, where U is the set of all triangle faces of a mesh, and \mathcal{A} is the set of all possible viewpoints that surround the mesh and are oriented towards it. Let S be a collection of subsets of \mathcal{A} , then, a set cover is a sub-collection S' of S such that every element in U is “covered” (=viewed by) at least one subset in S' . The goal is to find the smallest possible S' that covers all elements in U .*

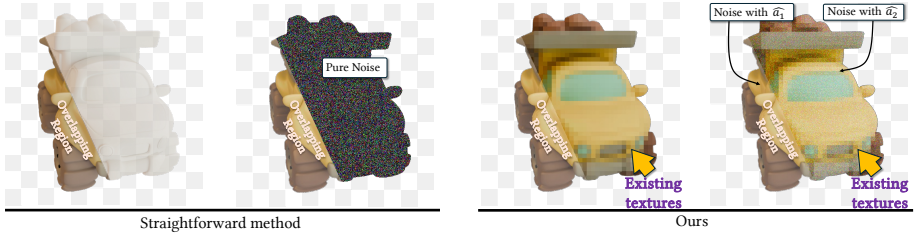


Fig. 9: The duplicate of Fig.4 for ease of reference The key difference between the proposed adaptive denoising strategy and the straightforward method used in the previous studies [4, 34]. In contrast to the straightforward that generates new textures from pure noise using an image inpainting diffusion model, ours injects noises to refine existing textures. We introduce how α_{t1} and α_{t2} are computed in Sec. 4.2’s adaptive denoising.

Theorem 1. Let $U = \{u_1, u_2, \dots, u_n\}$ be the universal set with n elements; let $S = \{S_1, S_2, \dots, S_m\}$ be the collection of subsets of U with m subsets. We define a binary variable x_j for each subset S_j in S where:

$$\begin{cases} x_j = 1 & \text{if } S_j \subset S' \\ x_j = 0 & \text{otherwise.} \end{cases} \quad (5)$$

The objective is to minimize the number of subsets selected in the set cover S' , which can be formulated as:

$$\min \sum_{j=1}^m x_j, \quad \text{s.t.} \quad \sum_{j: u_i \triangleleft S_j} x_j \geq 1, \quad \forall i \in \{1, 2, \dots, n\}, \forall j \in \{1, 2, \dots, m\}, \quad (6)$$

where $u_i \triangleleft S_j$ means a triangle face u_i is “covered” (=viewed) by at least one subset of viewpoints in S' .

Solution we solve the aforementioned problem using a heuristic greedy strategy and further relaxing the 0-1 integer programming problem of minimal coverage to a general optimization problem of maximizing the sum of areas of all covered faces. Specifically, we commence by sampling K candidate viewpoints from a spherical surface with a variable radius ranging from 1.0 to 1.4 (this assumes that the 3D mesh is normalized in the range of $[-1, 1]$). Following this, we assess the visibility between a viewpoint and each face of the mesh using ray-face intersection tests. We stipulate that the included angle in this interaction should be less than 45° . This results in an optimization that can be embarrassingly paralleled, typically clocking in at 1 to 2 seconds for the majority of models with a dense selection of K . We use $K = 8192$ for all our experiments.

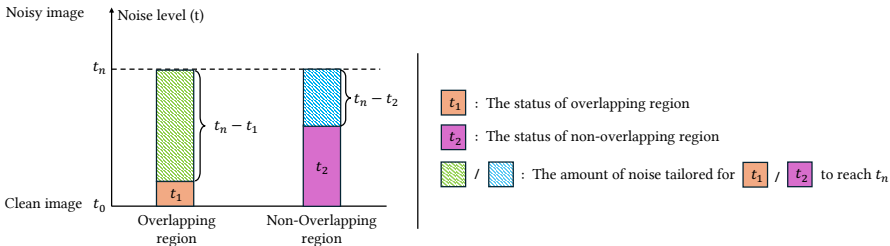


Fig. 10: The illustration demonstrates the essence of the proposed adaptive denoising strategy, explaining our intention to employ two distinct noise schedulers to diffuse the pixels in the overlapping and non-overlapping regions.

9 Additional Explanation of Adaptive Denoising

We have illustrated the essence of our proposed adaptive denoising strategy in Fig.4 of the main text. For ease of reference, we have replicated the figure and included it here (Fig. 9). We explain why we employ two noise schedulers, $\widehat{\alpha}_1$ and $\widehat{\alpha}_2$, for distinct applications to the overlapping and non-overlapping regions. We present our rationale behind naming the method "adaptive denoising" to the reader. The "Overlapping" region contains the co-visible pixels, whose colors are the outcomes of a previous adaptive denoising process, executed from a viewpoint adjacent to the current one. As illustrated in Fig. 10, we believe that the textures in the "Overlapping region" are in a state (denoted as t_1 in the figure) closer to the clean image, in terms of diffusion denoising. Conversely, the textures in the non-Overlapping region are in a state (denoted as t_2 in the figure) that is further from the clean image. In this scenario, we need to apply tailored noises (represented by $t_n - t_1$, $t_n - t_2$ in the figure) across the different regions (*i.e.*, overlapping and non-overlapping) to diffuse the pixels to a uniform level (denoted as t_n in the figure). We thus employ two noise schedulers ($\widehat{\alpha}_1$ and $\widehat{\alpha}_2$) to achieve this purpose, we calculate them using equations (2) and (3) written in the main text.

10 Comparison with Texfusion

We conduct a comparative analysis between our TexRO and Texfusion [2]. Since Texfusion’s code is not publicly available, we implemented its method ourselves, striving to replicate its original functionality accurately. We ensured the comparison was carried out in an identical experimental setting. Notably, Texfusion uses varying resolutions for UV maps for different samples, as mentioned in their paper (Sec.4.2.2). In contrast, our implementation uses an identical resolution for the UV maps for all the samples. We mimic the experimental details introduced in Texfusion’s paper, we utilize 24 viewpoints in the first stage and 9 viewpoints in the second stage. We conduct the comparison on Text2Tex-Data

Table 3: Evaluation results on the commonly used subset of Objaverse, *i.e.*, **Text2Tex-Data**, for 3D texture generation

Methods	FID ↓	KID ($\times 10^{-3}$) ↓	Runtime
TexFusion † [2]	37.91	7.40	6.2 min.
TexRO(Ours)	33.83	5.77	1 min.

Table 4: The results are computed on **Text2Tex-Cap3d**.

Method	FID ↓	KID ($\times 10^{-3}$) ↓
TexFusion † [2]	35.35	5.82
TexRO (Ours)	30.33	4.58

and **Text2Tex-Cap3D**. We do not use the samples used in the original Texfusion’s paper due to their cost. The quantitative comparison is shown in [Table 3](#) and [Table 4](#). It is seen that the proposed TexRO outperforms Texfusion by a good margin in terms of texture generalization quality and running time.